First-principles nonequilibrium Green's-function approach to transient photoabsorption: Application to atoms

E. Perfetto,[1,2] A.-M. Uimonen,[3] R. van Leeuwen,[4] and G. Stefanucci[2,5,*]

[1]*Dipartimento di Fisica, Università di Roma Tor Vergata, Via della Ricerca Scientifica 1, 00133 Rome, Italy*

[2]*INFN, Laboratori Nazionali di Frascati, Via E. Fermi 40, 00044 Frascati, Italy*

[3]*Department of Physics, Nanoscience Center, University of Jyväskylä, FIN 40014 Jyväskylä, Finland*

[4]*Department of Physics, Nanoscience Center, University of Jyväskylä, FIN 40014 Jyväskylä, Finland, and European Theoretical Spectroscopy Facility (ETSF)*

[5]*Dipartimento di Fisica, Università di Roma Tor Vergata, Via della Ricerca Scientifica 1, 00133 Rome, Italy, and European Theoretical Spectroscopy Facility (ETSF)*

(Received 15 July 2015; published 21 September 2015)

We put forward a first-principle nonequilibrium Green's-function (NEGF) approach to calculate the transient photoabsorption spectrum of optically thin systems. The method can deal with pump fields of arbitrary strength, frequency, and duration as well as overlapping and nonoverlapping pump and probe pulses. The electron-electron repulsion is accounted for by the correlation self-energy, and the resulting numerical scheme deals with matrices that scale quadratically with the system size. Two recent experiments, the first on helium and the second on krypton, are addressed. For the first experiment we explain the bending of the Autler-Townes absorption peaks with increasing pump-probe delay τ and relate the bending to the thickness and density of the gas. For the second experiment we find that sizable spectral structures of the pump-generated admixture of Kr ions are fingerprints of *dynamical correlation* effects, and hence they cannot be reproduced by time-local self-energy approximations. Remarkably, the NEGF approach also captures the retardation of the absorption onset of Kr^{2+} with respect to Kr^{1+} as a function of τ.

DOI: 10.1103/PhysRevA.92.033419 PACS number(s): 42.50.Md, 78.47.jb, 31.15.A−, 42.50.Hz

I. INTRODUCTION

Transient photoabsorption (TPA) spectroscopy has today become a popular technique to investigate the ultrafast dynamics of electrons and nuclei in atoms, molecules, and nanostructures [1–5]. A reliable physical interpretation of the TPA spectrum is inescapably linked to a reliable calculation of the probe-induced polarization in the pump-driven system. State-of-the-art calculations are based on the configuration interaction (CI) expansion of the time-evolved many-electron state. The time-dependent CI coefficients are either varied with respect to the probe field [6–11] or used to construct the dipole response function from the Lehmann representation [12–14], the latter approach being applicable only provided that the dressed pump and probe fields do not overlap [15]. However, the size of the arrays in CI calculations scale exponentially with the number of basis functions and the time step to achieve convergence is typically much smaller than the time step used in statistical approaches. Due to these numerical limitations the CI approach is confined to the study of rather small systems.

One possible statistical approach to TPA spectroscopy is time-dependent density functional theory (TDDFT) [16]. In TDDFT are the occupied single-particle wave functions that are propagated in time, and since they scale linearly with the number of basis functions TDDFT is suitable for studying much larger systems than those accessible by the CI. In the framework of the adiabatic local density approximation (ALDA), TDDFT has been recently and successfully applied to the study of TPA in small and medium-sized molecules [17] as well as to monitor the vibronic-mediated charge transfer in donor-acceptor complexes [18,19]. Still, ALDA functionals have drawbacks that could compromise the description of photoabsorption spectra even in *equilibrium* systems. For example, the ALDA misses correlation-induced spectral features like double-excitations [20,21] and long-range charge-transfer excitations [22–24]; it also provides a poor description of the energy-level alignment in metal/molecule interfaces [25,26] and of the Coulomb blockade phenomenon [27,28]. In this work we discover yet another correlation effect missed by the ALDA.

An alternative statistical approach to TDDFT is the many-body diagrammatic theory. Here the building blocks of the formalism are the nonequilibrium Green's functions (NEGF) [29–32] and correlation effects are included by a proper selection of self-energy diagrams. Double-excitations and other properties missed by the ALDA are within reach of diagrammatic theory already with basic self-energies. Recently, it has been shown that the TPA spectrum follows from the solution of a nonequilibrium Bethe-Salpeter equation (BSE) provided that the time scale of the pump-induced electron dynamics is much longer than the lifetime of the dressed probe field [33]. In general, however, for pump fields of arbitrary strength, frequency, and duration and/or for overlapping pump and probe pulses, the nonequilibrium BSE is inadequate and the full time propagation of the NEGF is unavoidable. Nevertheless, as the size of the arrays in NEGF calculations scales quadratically with the number of basis functions, this formalism also allows for extending the range of CI-accessible systems.

In this work we formulate a general first-principle NEGF scheme to TPA and apply it to reproduce the transient spectra of a thick helium gas [11] and of a krypton gas [34]. For helium we address the exponential damping of the probe-induced dipole

*gianluca.stefanucci@roma2.infn.it

and relate it to the thickness and density of the gas. We then provide the explanation of the bending of the Autler-Townes (AT) absorption peaks with increasing pump-probe delay. We also propose a useful formula for fitting the experimental TPA spectra. The krypton gas constitutes a more severe test for NEGF due to nontrivial correlation effects. We find that for a proper description of the (pump-generated) evolving admixture of Kr ions the self-energy should have *memory*. Static (or adiabatic) approximations like the Hartree-Fock (HF) or the Markovian approximations perform rather poorly, as only the spectrum of Kr^{1+} is visible. Instead, the TPA spectrum calculated using the (memory-dependent) second Born (2B) self-energy contains absorption lines attributable to excitations in the Kr^{1+} and Kr^{2+} ions. Remarkably, we are also able to reproduce the femtosecond retardation of the absorption onset of Kr^{2+} with respect to Kr^{1+} as a function of the pump-probe delay.

The paper is organized as follows. In Sec. II we relate the TPA spectrum to the microscopic quantum mechanical average of the transverse, probe-induced dipole wave propagating toward the detector. In Sec. III we put forward the NEGF approach to TPA and provide the explicit expression of the self-energy approximations implemented in this work. The helium gas is studied in Sec. IV. In Sec. V we extend the NEGF approach to deal with pump-induced ionization processes and then apply the extended approach to the study of krypton gas in Sec. VI. Summary and conclusions are drawn in Sec. VII.

II. TRANSIENT PHOTOABSORPTION SPECTRUM

We consider a gas of atoms or molecules perturbed by a strong time-dependent transverse electric field $\mathbf{E}(\mathbf{r}\,t)$ (pump) propagating along the unit vector $\mathbf{N}$ and a feeble time-dependent transverse electric field $\mathbf{e}(\mathbf{r}\,t)$ (probe) propagating along the unit vector $\mathbf{n}$ (see Fig. 1). The direction of propagation $\mathbf{N} \neq \mathbf{n}$ and in experiments the photodetector is positioned along the probe beamline. Let $\boldsymbol{\mathcal{E}}_p(\mathbf{r}\,t)$ be the component of the total electric field (external plus induced) propagating toward the detector and $\boldsymbol{\mathcal{E}}_p(t)$ be the value of $\boldsymbol{\mathcal{E}}_p(\mathbf{r}\,t)$ at the detector surface. Then the transmitted energy measured by the detector is

$$E_T = \mathcal{S}\frac{c}{2\pi}\int \frac{d\omega}{2\pi}|\tilde{\boldsymbol{\mathcal{E}}}_p(\omega)|^2, \tag{1}$$

with $\mathcal{S}$ the surface of the sample (assumed to be smaller than the laser-beam cross section). Here and in the following we use the convention that quantities with a tilde denote the Fourier transform of the corresponding time-dependent quantities. Replacing $\tilde{\boldsymbol{\mathcal{E}}}_p$ in Eq. (1) with the external probe field $\tilde{\mathbf{e}}$ we obtain the energy E_I of the incident probe beam.

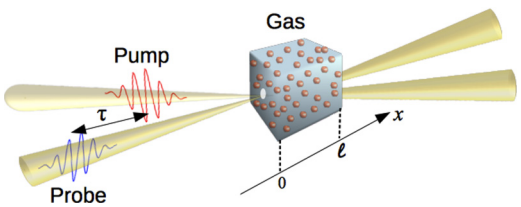

FIG. 1. (Color online) Schematic illustration of a pump-probe experiment.

The absorbed energy E_A is defined according to

$$\begin{aligned} E_A &\equiv E_I - E_T \\ &= \mathcal{S}\frac{c}{2\pi}\int \frac{d\omega}{2\pi}(|\tilde{\mathbf{e}}(\omega)|^2 - |\tilde{\boldsymbol{\mathcal{E}}}_p(\omega)|^2). \end{aligned} \tag{2}$$

By means of a spectrometer it is possible to measure the absorbed energy per unit frequency, i.e.,

$$\mathfrak{S}(\omega) = \mathcal{S}\frac{c}{2\pi}(|\tilde{\mathbf{e}}(\omega)|^2 - |\tilde{\boldsymbol{\mathcal{E}}}_p(\omega)|^2). \tag{3}$$

The quantity $\mathfrak{S}(\omega)$ is the TPA spectrum that we are interested in.

As both $\mathbf{E}$ and $\mathbf{e}$ are transverse fields we have $\mathbf{E}(\mathbf{r}\,t) = \mathbf{E}(X\,t)$ with $X = \mathbf{N}\cdot\mathbf{r}$ and $\mathbf{e}(\mathbf{r}\,t) = \mathbf{e}(x\,t)$ with $x = \mathbf{n}\cdot\mathbf{r}$. By definition $\boldsymbol{\mathcal{E}}_p$ too depends only on x, i.e., $\boldsymbol{\mathcal{E}}_p(\mathbf{r}\,t) = \boldsymbol{\mathcal{E}}_p(x\,t)$, since it is a transverse field propagating along $\mathbf{n}$. Without loss of generality we choose the coordinates of the boundaries of the sample in $x = 0$ and $x = \ell$, ℓ being the thickness of the gas (see Fig. 1). From Maxwell equations the relation between the total field and the incident probe field is

$$\boldsymbol{\mathcal{E}}_p(x\,t) = \mathbf{e}(x\,t) + \frac{2\pi}{c}\frac{d}{dt}\int_0^x dx'\mathbf{d}_p(x't), \tag{4}$$

where $\mathbf{d}_p(x\,t)$ is the component of the *probe-induced* dipole density propagating toward the detector [15]. Note that $\mathbf{d}_p(x\,t)$ vanishes for $x > \ell$; hence $\boldsymbol{\mathcal{E}}_p(\ell\,t)$ and $\boldsymbol{\mathcal{E}}_p(t)$ (the electric field at the detector surface) differ only by a time shift. This time shift is completely irrelevant for the calculation of the spectrum, so we can use either $\tilde{\boldsymbol{\mathcal{E}}}_p(\ell\,\omega)$ or $\tilde{\boldsymbol{\mathcal{E}}}_p(\omega)$ in Eq. (3).

Equation (4) connects the experimental outcome $\mathfrak{S}(\omega)$ to a quantum-mechanical average. Let us define $\mathbf{d}_p(x\,t)$ more rigorously. We denote by $|\Psi(\mathbf{r}\,t)\rangle$ the many-body state of an atom located in a volume element around $\mathbf{r}$ at time t when both pump and probe fields are present; similarly, $|\Psi_P(\mathbf{r}\,t)\rangle$ is the many-body state of the same atom when only the pump is present (probe-free state). The average of the atomic dipole operator $\hat{\mathbf{d}}(\mathbf{r})$ over these two states is $\mathbf{d}^{(\mathrm{at})}(\mathbf{r}\,t) = \langle\Psi(\mathbf{r}\,t)|\hat{\mathbf{d}}(\mathbf{r})|\Psi(\mathbf{r}\,t)\rangle$ and $\mathbf{d}_P^{(\mathrm{at})}(\mathbf{r}\,t) \equiv \langle\Psi_P(\mathbf{r}\,t)|\hat{\mathbf{d}}(\mathbf{r})|\Psi_P(\mathbf{r}\,t)\rangle$, respectively. The atomic probe-induced dipole is therefore

$$\mathbf{d}_p^{(\mathrm{at})}(\mathbf{r}\,t) \equiv \mathbf{d}^{(\mathrm{at})}(\mathbf{r}\,t) - \mathbf{d}_P^{(\mathrm{at})}(\mathbf{r}\,t). \tag{5}$$

For isotropic systems the probe-free $\mathbf{d}_P^{(\mathrm{at})}(\mathbf{r}\,t) = \mathbf{d}_P^{(\mathrm{at})}(X\,t)$ is a transverse field propagating along $\mathbf{N}$. Instead the atomic dipole $\mathbf{d}^{(\mathrm{at})}(\mathbf{r}\,t)$ is a transverse field propagating along all possible directions $k\mathbf{n} + K\mathbf{N}$, with k and K real numbers. To first order in $|\mathbf{e}|$ the component propagating along $\mathbf{N}$ ($k = 0$) is exactly $\mathbf{d}_P^{(\mathrm{at})}(X\,t)$. It is reasonable to expect that for $k \neq 0$ and for small $|\mathbf{e}|$ the dominant component of $\mathbf{d}^{(\mathrm{at})}(\mathbf{r}\,t)$ is the one propagating along the same direction $\mathbf{n}$ of the external probe. In this case the probe-induced atomic dipole $\mathbf{d}_p^{(\mathrm{at})}(\mathbf{r}\,t) = \mathbf{d}_p^{(\mathrm{at})}(x\,t)$ is a transverse field propagating along $\mathbf{n}$ and the function $\mathbf{d}_p$ appearing in Eq. (4) is simply $n^{(\mathrm{at})}\mathbf{d}_p^{(\mathrm{at})}$, $n^{(\mathrm{at})}$ being the density of the gas. We can therefore calculate $\mathbf{d}_p$ by performing a time propagation with the pump and probe, and another time propagation with only the pump, and then subtracting the resulting dipoles. Below we derive the basic equations to perform these calculations.

For an atom with unperturbed Hamiltonian $\hat{H}(\mathbf{r})$ the evolution of the state $|\Psi(\mathbf{r}\,t)\rangle$ is governed by the Schrödinger

equation

$$i\frac{d}{dt}|\Psi(\mathbf{r}\,t)\rangle = [\hat{H}(\mathbf{r}) + \boldsymbol{\mathcal{E}}(\mathbf{r}\,t)\cdot\hat{\mathbf{d}}(\mathbf{r})]|\Psi(\mathbf{r}\,t)\rangle, \tag{6}$$

where $\boldsymbol{\mathcal{E}}$ is the total electric field. We choose the pump and probe propagation directions such that $\mathbf{N}\cdot\mathbf{n}\approx 1$. Then $X = \mathbf{r}\cdot\mathbf{N} \simeq \mathbf{r}\cdot\mathbf{n} = x$ inside the sample and every $\mathbf{r}$-dependent quantity can be approximated with an x-only dependent quantity. In particular, the total field can be approximated as

$$\boldsymbol{\mathcal{E}}(x\,t) = \mathbf{E}(x\,t) + \mathbf{e}(x\,t) + \frac{2\pi}{c}n^{(\mathrm{at})}\frac{d}{dt}\int_0^x dx'\mathbf{d}^{(\mathrm{at})}(x'\,t). \tag{7}$$

For optically thin samples the dipole oscillations at two points x_1 and x_2 are time-shifted by an amount $|x_1 - x_2|/c$, which is much smaller than the inverse of the typical dipole frequencies. Therefore $\mathbf{d}^{(\mathrm{at})}(x'\,t) \simeq \mathbf{d}^{(\mathrm{at})}(t)$ is weakly dependent on x' inside the gas and we can approximate the integral in Eq. (7) with $x\mathbf{d}^{(\mathrm{at})}(t)$. The mathematical simplification brought about by this approximation is that every atom can be evolved separately. Consider the state $|\Psi(t)\rangle \equiv |\Psi(\ell\ y\ z\ t)\rangle$ of an atom at the interface in $x = \ell$ and let $\hat{H} \equiv \hat{H}(\ell\ y\ z)$ and $\hat{\mathbf{d}} \equiv \hat{\mathbf{d}}(\ell\ y\ z)$ be the atomic Hamiltonian and dipole operator. Then for $\mathbf{r} = (\ell\ y\ z)$ Eq. (6) reads

$$i\frac{d}{dt}|\Psi(t)\rangle = [\hat{H} + \boldsymbol{\mathcal{E}}(t)\cdot\hat{\mathbf{d}}]|\Psi(t)\rangle, \tag{8}$$

with

$$\boldsymbol{\mathcal{E}}(t) = \mathbf{E}(\ell\,t) + \mathbf{e}(\ell\,t) + \frac{2\pi\ell}{c}n^{(\mathrm{at})}\frac{d}{dt}\mathbf{d}^{(\mathrm{at})}(t) \tag{9}$$

and

$$\mathbf{d}^{(\mathrm{at})}(t) = \langle\Psi(t)|\hat{\mathbf{d}}|\Psi(t)\rangle. \tag{10}$$

Equations (8)–(10) form a close system of three coupled equations. The same equations could be solved for $\mathbf{e} = 0$ to obtain the probe-free atomic dipole $\mathbf{d}_P^{(\mathrm{at})}(t)$ and hence the probe-induced dipole $\mathbf{d}_p^{(\mathrm{at})}(t)$ in accordance with Eq. (5). Having $\mathbf{d}_p^{(\mathrm{at})}(t)$ we can calculate the probe-induced dipole density $\mathbf{d}_p(\ell\,t) = n^{(\mathrm{at})}\mathbf{d}^{(\mathrm{at})}(t)$ and, subsequently, the component of the electric field propagating toward the detector from Eq. (4), i.e.,

$$\boldsymbol{\mathcal{E}}_p(\ell\,t) = \mathbf{e}(\ell\,t) + \frac{2\pi\ell}{c}\frac{d}{dt}\mathbf{d}_p(\ell\,t). \tag{11}$$

Fourier transforming $\boldsymbol{\mathcal{E}}_p(\ell\,t)$ and $\mathbf{e}(\ell\,t)$, the TPA spectrum $\mathfrak{S}(\omega)$ in Eq. (3) follows:

$$\mathfrak{S}(\omega) = -2\mathrm{Im}[\omega\,\tilde{\mathbf{e}}^*(\ell\,\omega)\cdot\tilde{\mathbf{d}}_p(\ell\,\omega)] - \frac{2\pi\ell}{\mathcal{S}c}|\omega\,\tilde{\mathbf{d}}_p(\ell\,\omega)|^2. \tag{12}$$

The numerical solution of Eqs. (8)–(10) is impractical for heavy atoms or moderate-sized molecules. In the next section we describe a statistical approach which avoids solving the Schrödinger equation for the many-electron system. This approach is based on the NEGF [29–32] combined with the generalized Kadanoff-Baym Ansatz (GKBA) [35], and it has been successfully applied to electron gas [36,37], two-band model semiconductors [30,38–42], and, more recently, bulk silicon [43,44], Hubbard chains [45–47], and donor-acceptor junctions [48]. Here we extend it to perform first-principles simulations of laser-driven quantum systems.

III. NEGF APPROACH

We work in the formalism of second quantization and denote by $\hat{c}_{i\sigma}$ ($\hat{c}^\dagger_{i\sigma}$) the annihilation (creation) operator for an electron in the orbital $\varphi_i(\mathbf{r})$ with spin $\sigma = \uparrow,\downarrow$. Without loss of generality the basis $\{\varphi_i\}$ is taken orthonormal. The unperturbed Hamiltonian reads

$$\hat{H} = \sum_{\substack{ij\\\sigma}} h_{ij}\hat{c}^\dagger_{i\sigma}\hat{c}_{j\sigma} + \frac{1}{2}\sum_{\substack{ijmn\\\sigma\sigma'}} v_{ijmn}\hat{c}^\dagger_{i\sigma}\hat{c}^\dagger_{j\sigma'}\hat{c}_{m\sigma'}\hat{c}_{n\sigma}, \tag{13}$$

with $h_{ij} \equiv \int d\mathbf{r}\,\varphi_i^*(\mathbf{r})[-\frac{1}{2}\nabla^2 + V_{\mathrm{n}}(\mathbf{r})]\varphi_j(\mathbf{r})$ the one-electron integrals with nuclear potential V_{n} and

$$v_{ijmn} \equiv \int d\mathbf{r}\,d\mathbf{r}'\,\frac{\varphi_i^*(\mathbf{r})\varphi_j^*(\mathbf{r}')\varphi_m(\mathbf{r}')\varphi_n(\mathbf{r})}{|\mathbf{r}-\mathbf{r}'|} \tag{14}$$

the four-index Coulomb integrals. Similarly, the dipole operator reads

$$\hat{\mathbf{d}} = \sum_{\substack{ij\\\sigma}} \mathbf{d}_{ij}\hat{c}^\dagger_{i\sigma}\hat{c}_{j\sigma}, \tag{15}$$

with $\mathbf{d}_{ij} \equiv \int d\mathbf{r}\,\varphi_i^*(\mathbf{r})\mathbf{r}\varphi_j(\mathbf{r})$ the matrix elements of the dipole vector. The time-dependent average of the atomic dipole, see Eq. (10), is therefore

$$\mathbf{d}^{(\mathrm{at})}(t) = \sum_{\substack{ij\\\sigma}} \mathbf{d}_{ij}\langle\Psi(t)|\hat{c}^\dagger_{i\sigma}\hat{c}_{j\sigma}|\Psi(t)\rangle. \tag{16}$$

Let us introduce the evolution operator $\mathcal{U}(t,t_0)$ from a time t_0 when the system is unperturbed to an arbitrary time t. Then $|\Psi(t)\rangle = \mathcal{U}(t,t_0)|\Psi_0\rangle$, with $|\Psi_0\rangle$ the state of the unperturbed system. To distinguish the Heisenberg from the Schrödinger picture we add the subscript "H" to the operator $\hat{O}(t)$ in the Schrödinger picture, $\hat{O}_H(t) \equiv \mathcal{U}(t_0,t)\hat{O}(t)\mathcal{U}(t,t_0)$. The lesser ($G^<$) and greater ($G^>$) Green's functions are defined according to

$$G^<_{ij}(t,t') = i\langle\Psi_0|\hat{c}^\dagger_{j\sigma,H}(t')\hat{c}_{i\sigma,H}(t)|\Psi_0\rangle, \tag{17a}$$

$$G^>_{ij}(t,t') = -i\langle\Psi_0|\hat{c}_{i\sigma,H}(t)\hat{c}^\dagger_{j\sigma,H}(t')|\Psi_0\rangle \tag{17b}$$

and have the property

$$G^{\lessgtr}_{ij}(t,t') = -[G^{\lessgtr}_{ji}(t',t)]^*, \tag{18}$$

implying that from $G^{\lessgtr}$ with times $t \geqslant t'$ or $t \leqslant t'$ we can reconstruct the entire $G^{\lessgtr}$. In this work we consider spin-compensated systems with no spin-orbit interaction; hence $G^{\lessgtr}$ takes the same value for $\sigma = \uparrow,\downarrow$. The NEGF formalism, however, is not limited to this case and it can easily be generalized to Hamiltonians that are not diagonal in spin space. From $G^<$ at equal times we can calculate the time-dependent average of any one-body operator; in particular, the atomic dipole in Eq. (16) reads $\mathbf{d}^{(\mathrm{at})}(t) = -2i\sum_{ij}\mathbf{d}_{ij}G^<_{ji}(t,t)$.

The lesser and greater Green's functions satisfy nonlinear integro-differential equations known as the Kadanoff-Baym equations (KBEs) [29–32]. At present the numerical solution of the KBEs for inhomogeneous systems is possible only for moderate-sized basis sets [49–55], and still the CPU time is of the order of a few days for a propagation of $\sim 10^3$ time steps

and $\sim 10^1$ basis functions. Considering that a TPA spectrum typically requires 10^4 time steps for every delay between the pump and the probe pulses, the KBEs are not feasible in this context. A way to drastically reduce the computational effort consists in making the GKBA [35]:

$$G^<(t,t') = -G^{\rm R}(t,t')\rho(t') + \rho(t)G^{\rm A}(t,t'), \quad (19a)$$

$$G^>(t,t') = G^{\rm R}(t,t')\bar\rho(t') - \bar\rho(t)G^{\rm A}(t,t'). \quad (19b)$$

In these equations $G^{\rm R}(t,t') = [G^{\rm A}(t',t)]^\dagger$ is the retarded Green's function and $\rho(t) = -iG^<(t,t) = 1 - \bar\rho(t) = 1 - iG^>(t,t)$ is the one-particle density matrix (the quantity of interest for the calculation of the atomic dipole). The GKBA is exact in the HF approximation and it is expected to be accurate in systems with well-defined quasiparticles (see Ref. [48] for a recent discussion). From the KBEs we can easily derive (see the Appendix), the equation of motion for ρ (in matrix form),

$$-i\frac{d}{dt}\rho(t) + [h_{\rm HF}(t),\rho(t)] = iI(t) - {\rm H.c.}, \quad (20)$$

where the HF single-particle Hamiltonian reads

$$h_{{\rm HF},ij}(t) = h_{ij} + \boldsymbol{\mathcal{E}}(t)\cdot\mathbf{d}_{ij} + \sum_{mn} w_{imnj}\rho_{nm}(t), \quad (21)$$

with

$$w_{imnj} \equiv 2v_{imnj} - v_{imjn}, \quad (22)$$

and the collision integral reads (in matrix form)

$$I(t) = \int_{-\infty}^{t} dt'[\Sigma^<(t,t')G^>(t',t) + \Sigma^>(t,t')G^<(t',t)]. \quad (23)$$

The correlation self-energy $\Sigma^{\lessgtr}$ appearing in Eq. (23) is a functional of $G^<$ and $G^>$, which, in turn, are functionals of ρ through the GKBA. Thus, Eq. (20) is a closed nonlinear integrodifferential equation for ρ once we specify the functional form of the self-energy and the retarded Green's function.

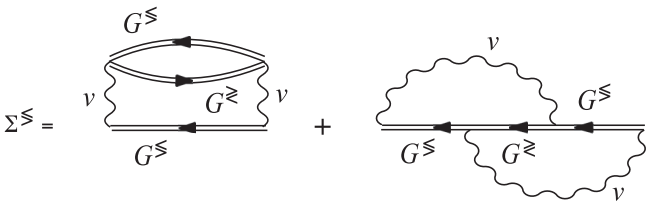

FIG. 2. Diagrammatic representation of the 2B self-energy. Wiggly lines denote the Coulomb interaction v.

In this work we present results obtained using the 2B self-energy

$$\Sigma^{\lessgtr}_{ij}(t,t') = \sum_{\substack{nm\\pq\\sr}} v_{irpn}w_{mqsj}G^{\lessgtr}_{nm}(t,t')G^{\lessgtr}_{pq}(t,t')G^{\gtrless}_{sr}(t',t), \quad (24)$$

whose diagrammatic representation is shown in Fig. 2. For the retarded Green's function we consider

$$G^{\rm R}(t,t') = -i\theta(t-t')\,T[e^{-i\int_{t'}^{t} d\bar t\, h_{\rm HF}(\bar t)}], \quad (25)$$

where T is the time-ordering operator. In Ref. [48] we discussed how to include correlation effects (beyond HF) in $G^{\rm R}$ and showed their importance in quantum transport calculations. For the finite systems analyzed here, however, we found that the HF $G^{\rm R}$ of Eq. (25) is accurate enough. Similar findings were recently found in strongly correlated systems as well [56,57]. In addition to the simplicity of Eq. (25), the use of an HF $G^{\rm R}$ within the NEGF + GKBA scheme guarantees the satisfaction of all basic conservation laws [47].

We emphasize that the equation of motion for ρ is an equation with memory since the evaluation of the collision integral at time t involves the density matrix at all times $t' \leqslant t$. Using the GKBA expression for the lesser and greater Green's function the collision integral can be rewritten as

$$I_{ik}(t) = \sum_{\substack{nm\\pq\\sr}}\sum_{j} v_{irpn}w_{mqsj}\int_{-\infty}^{t} dt'[(G^{\rm R}(t,t')\rho(t'))_{nm}(G^{\rm R}(t,t')\rho(t'))_{pq}(\bar\rho(t')G^{\rm A}(t',t))_{sr}(\bar\rho(t')G^{\rm A}(t',t))_{jk}$$
$$+ (G^{\rm R}(t,t')\bar\rho(t'))_{nm}(G^{\rm R}(t,t')\bar\rho(t'))_{pq}(\rho(t')G^{\rm A}(t',t))_{sr}(\rho(t')G^{\rm A}(t',t))_{jk}]. \quad (26)$$

From Eq. (26) it is evident that the computational cost scales quadratically with the maximum propagation time. The quadratic scaling can be reduced to a linear scaling if the collision integral is evaluated in the Markov approximation. The Markov approximation consists in neglecting memory effects by replacing the pair $\rho(t')$ and $\bar\rho(t')$ with the pair $\rho(t)$ and $\bar\rho(t)$, and in using the *equilibrium* HF retarded Green's function $G^{\rm R}(t,t') = -i\theta(t-t')\exp[-ih^{\rm eq}_{\rm HF}(t-t')]$, with $h^{\rm eq}_{\rm HF}$ the HF single-particle Hamiltonian of the equilibrium system. In this case the integral over t' can be done analytically and the collision integral becomes a quartic polynomial in $\rho(t)$. Thus the equation of motion for ρ reduces to a nonlinear differential equation. In the next sections we benchmark the Markov approximation against CI and full NEGF + GKBA simulations.

IV. HELIUM

In this section we simulate the TPA spectrum of helium atoms recently measured in Ref. [11]. Helium is among one of the most studied systems in the context of TPA [6,8,11,58–63], and due to the limited number of electrons, CI simulations are very accurate. From our point of view helium provides an extremely useful platform for benchmarking the

NEGF + GKBA methodology. The gas of He atoms is perturbed by a near-infrared (NIR) transverse pump pulse $\mathbf{E}(\ell\, t) = (E(t),0,0)$ with $E(t) = E_0 \sin^2(\pi t/\Delta_P)\sin(\omega_P t)$ for $0 < t < \Delta_P$. The experimental pump intensity is $\mathcal{I}_0 = 6 \times 10^{12}\mathrm{W/cm^2}$, which corresponds to an electric field $E_0 = \sqrt{2\mathcal{I}_0/c\epsilon_0} = 6.6 \times 10^9$ V/m, the duration of the pump pulse is $\Delta_P \sim 15$ fs, and the NIR frequency, $\omega_P \sim 0.57$ eV, is slightly detuned from the $2s$-$2p$ resonance. Thus, the pump alone does not perturb the equilibrium state of the He atoms as both the $2s$ and the $2p$ levels are empty. The situation changes if the probe pulse arrives first. In the experiment the probe field is an ultrashort pulse, $\mathbf{e}(\ell\, t) = (e(t),0,0)$, with $e(t) = e_0 \sin^2(\pi(t-\tau)/\Delta_p)\sin(\omega_p(t-\tau))$ for $\tau < t < \tau + \Delta_p$. The probe pulse has duration $\Delta_p \sim 0.5$ fs, it is centered at frequency $\omega_p = 22$ eV, and it has an intensity $\mathcal{I}_0 \sim 10^9\mathrm{W/cm^2}$, which corresponds to an electric field $e_0 = 8.6 \times 10^7$ V/m. The density $n^{(\mathrm{at})}$ can been deduced from the pressure P of the gas: $n^{(\mathrm{at})} = P/(K_B T)$, with K_B the Boltzmann constant. The experimental estimate of P varies in the range 10–240 mb, implying that at room temperature $n^{(\mathrm{at})}$ varies in the range 5.8×10^{16} to 2.4×10^{17} $\mathrm{cm^{-3}}$. Finally, we observe that the experimental thickness ($1\ \mu\mathrm{m} \div 1$ mm) is much larger than the wavelength of the laser pulses (optically thick samples). To deal with these thicknesses, we propose the approximation $\int_0^\ell dx' \mathbf{d}^{(\mathrm{at})}(x'\, t) \simeq \ell_{\mathrm{eff}} \mathbf{d}^{(\mathrm{at})}(\ell\, t)$, where the effective thickness $\ell_{\mathrm{eff}} < \ell$ can be used as a fitting parameter. As we shall see this approximation well captures the effects of screening in the TPA spectrum of a thick helium gas.

We obtained the one- and two-electron integrals as well as the dipole matrix elements from the SMILES package [64,65] using the VB2 Slater-type orbital basis, consisting of 15 basis functions. We performed CI time propagations as well as NEGF + GKBA propagations in the HF ($\Sigma = 0$), 2B, and Markovian 2B approximations. As a general comment we observe that the time step to achieve convergence with the CI is about an order of magnitude smaller than with the NEGF + GKBA, thereby the CI requires about 10 times more time steps than the NEGF + GKBA to have the same frequency resolution.

In Fig. 3 we compare the TPA spectra in the four schemes for a gas with $\ell_{\mathrm{eff}} = 0.16$ mm and density $n^{(\mathrm{at})} = 2.4 \times 10^{17}$ $\mathrm{cm^{-3}}$. The spectra are obtained by a fast Fourier transform of $\mathbf{d}_p^{(\mathrm{at})}(t)$ calculated using a time step $\Delta t = 0.0012$ fs and 40 000 time steps in the CI and $\Delta t = 0.006$ fs and 7500 time steps in the NEGF + GKBA. In the CI (top left), the equilibrium peak of the $1s$-$2p$ transition occurs at a frequency of 21.1 eV, in agreement with the experiment, whereas the $1s$-$3p$ transition is not accurate. Nevertheless, as our interest is in the evolution of the $1s$-$2p$ transition as the pump-probe delay is varied, the VB2 basis is suitable for our purposes. The overall shape of the CI TPA spectrum is well reproduced by all NEGF approximations; see, e.g., the size of the splitting and the relaxation toward the equilibrium spectrum. The only relevant difference is a uniform frequency shift. We also observe that the intensity of the equilibrium peak grows monotonically with decreasing τ (no coherent oscillations), a feature in common with the experiment. In HF (see top right), the energy of the $1s$-$2p$ transition is overestimated. The inclusion of correlation effects at the 2B level (see bottom left) counteracts this overestimation, although the correction is too large. Interestingly the Markovian 2B approximation (see bottom right) does not change the position of the HF peak, a result which points to the importance of memory effects (see also Sec. VI).

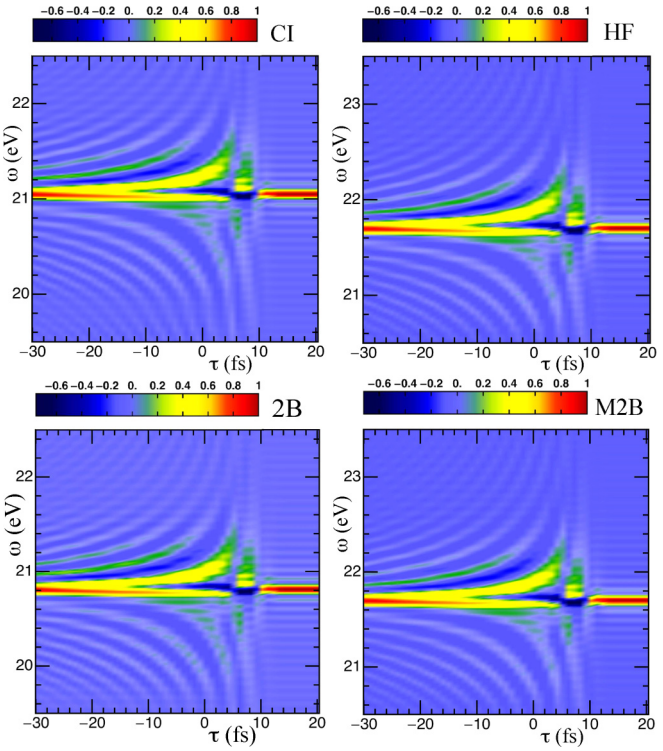

FIG. 3. (Color online) Density plot of the TPA spectrum (normalized to the maximum height) of a helium gas with $\ell_{\mathrm{eff}} = 0.16$ mm and density $n^{(\mathrm{at})} = 2.4 \times 10^{17}$ $\mathrm{cm^{-3}}$. Pump and probe pulses are given in the text. Results obtained with the CI (top left), HF (top right), 2B (bottom left), and Markovian 2B (MTB; bottom right).

The performance of the NEGF + GKBA approach is satisfactory for larger thicknesses too. In Fig. 4 we compare the TPA spectrum for $\ell_{\mathrm{eff}} = 1.6$ mm and density $n^{(\mathrm{at})} = 2.4 \times 10^{17}$ $\mathrm{cm^{-3}}$ in the four schemes. The fast Fourier transform of $\mathbf{d}_p^{(\mathrm{at})}(t)$ has been performed with $\Delta t = 0.0012$ fs and 10 000 time steps in the CI and $\Delta t = 0.006$ fs and 1500 time steps in the NEG + GKBA. Again, all main features of the CI spectrum are well reproduced. The width of the absorption peaks is larger compared to that in Fig. 3 since the lifetime of the probe-induced dipole is about an order of magnitude shorter.

Let us now come to the physical interpretation of the TPA spectrum. For small τ the equilibrium peak of the $1s$-$2p$ transition undergoes an AT splitting since the $2p$ and $2s$ levels are mixed by the pump field. The asymmetry of the AT intensities is due to the fact that ω_P is not exactly tuned at the $2s$-$2p$ resonance. For a pump of finite duration to generate an AT splitting the probe-induced dipole *must* decay in a time window $W \lesssim \Delta_P$. In fact, the pump affects the oscillations of $\mathbf{d}_p(t)$ only in a time window Δ_P, hence it cannot change the position of the peaks of $\tilde{\mathbf{d}}_p(\omega)$ if $W \gg \Delta_P$ [15]. As the time evolution is unitary and the system is finite, the damping mechanism of the dipole moment is not driven by electron-electron scattering. The damping mechanism does not have its

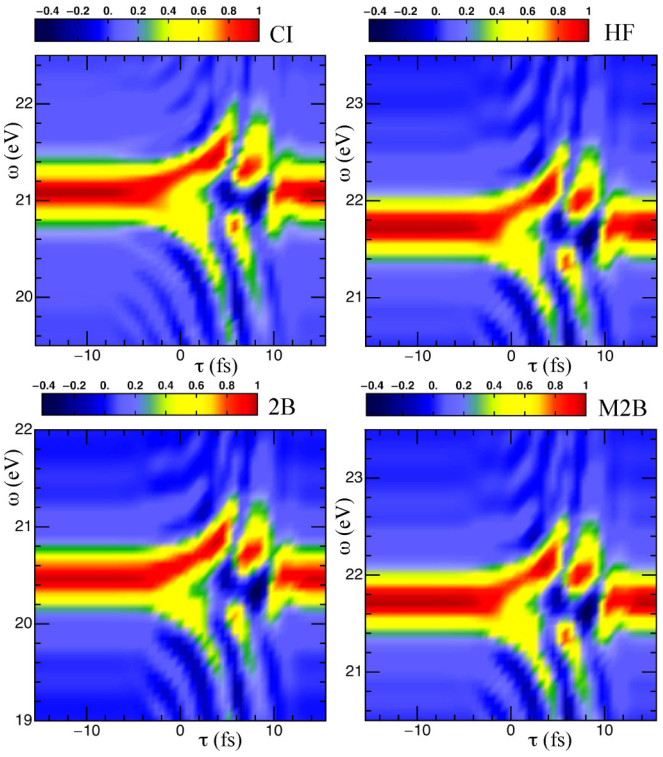

FIG. 4. (Color online) Density plot of the TPA spectrum (normalized to the maximum height) of a helium gas with $\ell_{\rm eff} = 1.6$ mm and density $n^{(\rm at)} = 2.4 \times 10^{17}$ cm^{-3}. Pump and probe pulses are given in the text. Results obtained with the CI (top left), HF (top right), 2B (bottom left), and Markovian 2B (M2B; bottom right).

origin in the radiative decay either (in He, relaxation through radiative decay is no shorter than hundreds of femtoseconds). We explain the origin of the damping mechanism in Sec. IV A. Here we address a different issue, i.e., the bending of the AT absorption peaks as τ decreases and the possible formation of a subsplitting structure.

Consider a three-level He model with basis functions $1s$, $2s$, $2p$ in the oscillating state induced by the probe. If the probe is switched off at $t = 0$, then for $t > 0$ the probe-induced dipole (along the x component) is $d_p(t) = d_0 \sin(\omega_0 t)$, where ω_0 is the energy of the $1s$-$2p$ transition and $d_0 = d_{x,1s2p}$ is the dipole matrix element. At time $-\tau > 0$ we switch on a pump field $E(t) = E_0 e^{-\gamma_P(t+\tau)} \sin(\omega_P(t+\tau))$, of duration $\Delta_P \sim 1/\gamma_P$, which couples the $2s$ and $2p$ levels. We choose ω_P in resonance with the energy of the $2s$-$2p$ transition and work in the rotating-wave approximation. Then for times $t > -\tau$ we find [15] $d_p(t) = d_0 \sin(\omega_0 t) \cos(E_0 d_0 \frac{1-e^{-\gamma_P(t+\tau)}}{\gamma_P})$ (we assumed for simplicity that the matrix element $d_{x,2s2p} = d_0$). Collecting these results and introducing an exponential damping $\gamma \sim 1/W$ (the origin of which is explained in Sec. IV A), we can write

$$\frac{d_p(t)}{d_0} = e^{-\gamma t} \sin(\omega_0 t) \times \begin{cases} 1, & t < -\tau, \\ \cos\left(E_0 d_0 \frac{1-e^{-\gamma_P(t+\tau)}}{\gamma_P}\right), & t > -\tau, \end{cases} \tag{27}$$

and $d_p(t) = 0$ for $t < 0$ (before the probe). This equation clearly illustrates the behavior previously discussed. For $t > -\tau + 1/\gamma_P$ the cosine is essentially constant. Thus, if $\gamma \ll \gamma_P$ (hence $W \gg \Delta_P$), then the pump modifies the $\sin(\omega_0 t)$ profile only in the time window $(-\tau, -\tau + 1/\gamma_P)$, too short to change the position of the peaks in $\pm\omega_0$ of the Fourier transform $\tilde{d}_p(\omega)$. Let us now consider the opposite limit, $\gamma \gg \gamma_P$ (hence $W \ll \Delta_P$). For all times t smaller than $1/\gamma$ (after this time the dipole is exponentially small) we can approximate the cosine with $\cos(E_0 d_0 (t+\tau))$. In this approximation the Fourier transform $\tilde{d}_p(\omega)$ has a simple analytic form and for, e.g., $\omega \simeq \omega_0 + E_0 d_0$, we find

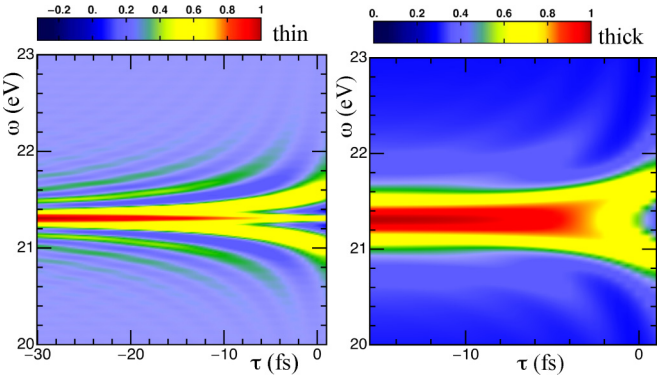

FIG. 5. (Color online) Density plot of $-\omega \mathrm{Im}[\tilde{d}_p(\omega)]/d_0$, with $\tilde{d}_p$ the Fourier transform of the function d_p in Eq. (27), for $\omega_0 = 21.3$ eV, $E_0 d_0 = 0.5$ eV, $\gamma_P = 0.41$ eV and for $\gamma = 0.21$ eV (left) and $\gamma = 1.37$ eV (right).

$$-\mathrm{Im}[\tilde{d}_p(\omega)] \simeq \frac{e^{-\gamma\tau}}{4} \frac{\gamma \cos(\bar{\omega}\tau) + (\bar{\omega} - E_0 d_0)\sin(\bar{\omega}\tau)}{(\bar{\omega} - E_0 d_0)^2 + \gamma^2}, \tag{28}$$

with $\bar{\omega} \equiv \omega - \omega_0$. The denominator of Eq. (28) has a minimum in $\bar{\omega} = E_0 d_0$ which is *independent* of τ. However, the maximum of $-\mathrm{Im}[\tilde{d}_p(\omega)]$ does not coincide with the minimum of the denominator as τ decreases from 0. For small negative τ the maximum occurs at frequencies $\bar{\omega} \simeq E_0 d_0 (1 + \tau\gamma/2) < E_0 d_0$. This explains the bending of the AT absorption peaks (a similar analysis can be done for frequencies $\omega \simeq \omega_0 - E_0 d_0$).

Noteworthily, the full Fourier transform of the dipole in Eq. (27) yields spectra that resemble very closely those in Figs. 3 and 4. In Fig. 5 we display the density plot of $-\omega \mathrm{Im}[\tilde{d}_p(\omega)] \propto \mathfrak{S}(\omega)$ for $\omega_0 = 21.3$ eV, $E_0 d_0 = 0.5$ eV, and $\gamma_P = 0.41$ eV (corresponding to a duration $\Delta_P \sim 10$ fs) and for $\gamma = 0.21$ eV (left; compare with Fig. 3) and $\gamma = 1.37$ eV (right; compare with Fig. 4). Equation (27) does therefore provide a convenient analytic parametrization of experimental TPA spectra. For longer pumps Eq. (27) predicts the formation of a subsplitting structure as well. In Fig. 6 we show the TPA spectrum as a function of the dipole lifetime $1/\gamma$ at delay $\tau = 0$ for $\omega_0 = 21.3$ eV, $E_0 d_0 = 0.2$ eV, and $\gamma_P = 0.125$ eV (corresponding to a duration $\Delta_P \sim 33$ fs). In addition to the AT peaks at $\omega_0 \pm E_0 d_0$, two extra peaks emerge, in agreement with recent experiments on a thick helium gas perturbed by an NIR pump of duration 33 fs [66]. We point out that the number of extra peaks increases with increasing AT splitting (hence with increasing intensity of the NIR pulse), a prediction which could be easily checked experimentally.

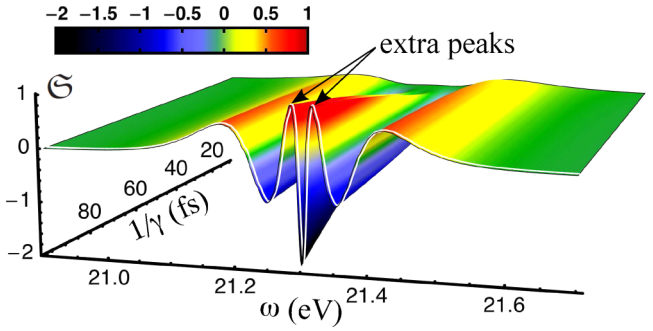

FIG. 6. (Color online) Three-dimensional plot of $-\omega \mathrm{Im}[\tilde{d}_p(\omega)]/d_0$ (normalized to the maximum height), with $\tilde{d}_p$ the Fourier transform of the function d_p in Eq. (27), as a function of the dipole lifetime $1/\gamma$ at delay $\tau = 0$ for $\omega_0 = 21.3$ eV, $E_0 d_0 = 0.2$ eV, $\gamma_P = 0.125$ eV. Arrows indicate the extra peaks discussed in the text.

A. Damping in closed systems with unitary evolution

The damping of the probe-induced dipole in helium gas has been systematically investigated both numerically and experimentally in Ref. [66]. Here we provide a transparent explanation based on the analytic solution of the Schrödinger equation, (8), for a simple two-level model with two-particle states $|1s^2\rangle$ and $|1s2p_x\rangle$. We take the equilibrium Hamiltonian $\hat{H}$ diagonal on this basis and let ϵ_1 and ϵ_2 be the corresponding eigenenergies. We denote by $d_0 = \langle 1s^2|\hat{d}_x|1s2p_x\rangle$ the x component of the dipole matrix element and write the dressed probe field along x in accordance with Eq. (11), i.e., $\mathcal{E}_p(t) = e(t) + \alpha \dot{d}(t)$, where $\alpha = 2\pi \ell_{\mathrm{eff}} n^{(\mathrm{at})}/c > 0$ and $d(t) = \langle \Psi(t)|\hat{d}_x|\Psi(t)\rangle$. Expanding the time-dependent two-particle state as $|\Psi(t)\rangle = c_1(t)|1s^2\rangle + c_2(t)|1s2p_x\rangle$, we find

$$i\dot{c}_1(t) = \epsilon_1 c_1(t) + d_0 \mathcal{E}_p(t) c_2(t), \tag{29a}$$

$$i\dot{c}_2(t) = \epsilon_2 c_2(t) + d_0 \mathcal{E}_p(t) c_1(t). \tag{29b}$$

For any real $\mathcal{E}_p$ the time evolution of the coefficients c_1 and c_2 is unitary. The expression of the time-dependent dipole in terms of c_1 and c_2 reads $d(t) = 2d_0 \mathrm{Re}[c_1^*(t)c_2(t)]$. We can get a differential equation for d if we introduce two more real functions $g(t) = \mathrm{Im}[c_1^*(t)c_2(t)]$ and $f(t) = |c_1(t)|^2 - |c_2(t)|^2$. It is a matter of simple algebra to show that after the probe (hence $e(t) = 0$) these three functions satisfy the system

$$\dot{f}(t) = -2d_0 \alpha g(t) \dot{d}(t), \tag{30a}$$

$$\dot{g}(t) = -\frac{\omega_0}{2d_0} d(t) + \alpha d_0 f(t) \dot{d}(t), \tag{30b}$$

$$\dot{d}(t) = 2d_0 \omega_0 g(t), \tag{30c}$$

where we have introduced $\omega_0 = \epsilon_1 - \epsilon_2$. Taking the time derivative of Eq. (30c) and using Eq. (30b) we find

$$\ddot{d}(t) + \omega_0^2 d(t) - 2\alpha d_0^2 \omega_0 f(t) \dot{d}(t) = 0. \tag{31}$$

With the help of Eq. (30c) we rewrite Eq. (30a) as $\dot{f}(t) = -\frac{\alpha}{\omega_0} \dot{d}^2(t)$. Therefore $f(t)$ is a monotonically decreasing function of time, and by definition, it is bounded between -1 and 1. This implies that $\lim_{t\to\infty} f(t) = f_\infty \in (-1,1)$. If f_∞ were positive, then the long-time solution of Eq. (31) would be an oscillatory function with an exponentially increasing amplitude, in contradiction with the fact that $d(t) \in (d_0, -d_0)$. We conclude that the limiting value $f_\infty \in (-1,0)$ independently of the initial condition. Consequently, for large t the function $d(t)$ oscillates at frequency ω_0 with an amplitude decaying as $e^{-\gamma t}$, where $\gamma = 2\alpha d_0^2 \omega_0 |f_\infty|$. Our analysis does explain the physical origin of the damping as well as the dependence of γ on the thickness and density of the gas. In fact, $\gamma \propto \alpha \propto \ell_{\mathrm{eff}} n^{(\mathrm{at})}$; therefore the larger the thickness and/or the density is and the more rapidly the amplitude of the dipole oscillations decays.

V. PUMP-INDUCED IONIZATION

In this Section we extend the NEGF + GKBA formalism to deal with ionization processes induced by the pump. For this purpose it is convenient to work with the HF orbitals. Let ρ^{eq} be the equilibrium density matrix and

$$h^{\mathrm{eq}}_{\mathrm{HF},ij} = h_{ij} + \sum_{mn} w_{imnj} \rho^{\mathrm{eq}}_{nm} \tag{32}$$

the equilibrium HF Hamiltonian in the original basis. The HF orbitals $\psi_\mu(\mathbf{r}) = \sum_i a_i^\mu \varphi_i(\mathbf{r})$ diagonalize both $h^{\mathrm{eq}}_{\mathrm{HF}}$ and ρ^{eq} and are orthonormal. To distinguish the HF basis from the original basis we use Greek letters to label the former. We have

$$h^{\mathrm{eq}}_{\mathrm{HF},\mu\nu} = \delta_{\mu\nu} \epsilon_\mu \tag{33}$$

and $\rho^{\mathrm{eq}}_{\mu\nu} = \delta_{\mu\nu} n_\mu$, where $n_\mu = 1$ if $\epsilon_\mu < \epsilon_{\mathrm{F}} < 0$ and $n_\mu = 0$ otherwise, ϵ_{F} being the Fermi energy.

In finite systems like atoms and molecules the HF orbitals with $\epsilon_\mu > 0$ are states in the continuum. These are the states that get occupied by the photoelectron in a ionization process. We assume that the Coulomb interaction between photoelectrons and bound electrons is negligible and set to zero the two-electron integrals $v_{\mu\nu\alpha\beta}$ with at least one of the four indices in the continuum (this amounts to neglecting Auger transitions). Then the self-energy has nonvanishing matrix elements only between bound states. In the Appendix we prove that the equation of motion for the density matrix with both indices in the bound sector reads

$$-i\frac{d}{dt}\rho(t) + [h_{\mathrm{HF}}(t), \rho(t)] = i[I(t) + I_{\mathrm{ion}}(t)] - \mathrm{H.c.} \tag{34}$$

In Eq. (34) every matrix has indices running over the bound states. The integral I_{ion} accounts for the pump-induced ionization (since $\mathrm{Tr}[I_{\mathrm{ion}} + \mathrm{H.c.}] \neq 0$ the number of bound electrons is not conserved) and it is calculated as in Eq. (23) except that the correlation self-energy is replaced by the ionization self-energy Σ_{ion}. The latter has a vanishing lesser part and a greater part given by (see the Appendix)

$$\Sigma^{>}_{\mathrm{ion}}(t,t') = \sum_{ij} \mathcal{E}_i(t) \sigma^{ij}(t-t') \mathcal{E}_j(t'). \tag{35}$$

Here $\mathcal{E}_i$ is the ith component of the electric field $\boldsymbol{\mathcal{E}} = (\mathcal{E}_x, \mathcal{E}_y, \mathcal{E}_z)$ and the tensor

$$\sigma^{ij}_{\mu\nu}(t-t') = -i \sum_{\alpha\in c} d_{i,\mu\alpha}\, e^{-i\epsilon_\alpha (t-t')}\, d_{j,\alpha\nu}, \tag{36}$$

where d_i is the ith component of the vector of matrices $\mathbf{d} = (d_x, d_y, d_z)$ and the sum over α runs in the continuum. In Fourier space

$$\tilde{\sigma}^{ij}_{\mu\nu}(\omega) = -2\pi i \sum_{\alpha\in c} d_{i,\mu\alpha}\,\delta(\omega-\epsilon_\alpha)\,d_{j,\alpha\nu} \approx 2i \sum_{\alpha\in c} d_{i,\mu\alpha}\mathrm{Im}\left[\frac{1}{\omega-\epsilon_\alpha+i\eta}\right]d_{j,\alpha\nu}, \quad (37)$$

where η is a positive constant of the order of the level spacing of the continuum states. Typically the ionization is caused by the action of a pump pulse with a Fourier transform peaked around some frequency ω_P (larger than the ionization energy of the system). Therefore, $\Sigma^{>}_{\rm ion}$ is dominated by those terms in $\sigma(t-t')$ that oscillate at frequency $\epsilon_\alpha \simeq \omega_P$. By virtue of this observation we implement a time-local approximation,

$$\tilde{\sigma}^{ij}_{\mu\nu}(\omega) \approx \tilde{\sigma}^{ij}_{\mu\nu}(\omega_P), \quad (38)$$

which implies $\sigma^{ij}_{\mu\nu}(t-t') = \tilde{\sigma}^{ij}_{\mu\nu}(\omega_P)\delta(t-t')$. Substituting this result into Eq. (35) yields

$$\Sigma^{>}_{\rm ion}(t,t') = -i\delta(t-t')\Gamma_{\mu\nu}(t), \quad (39)$$

where

$$\Gamma_{\mu\nu}(t) = i\sum_{ij}\mathcal{E}_i(t)\tilde{\sigma}^{ij}_{\mu\nu}(\omega_P)\mathcal{E}_j(t) \quad (40)$$

is a self-adjoint positive-definite matrix for all times t.

The time-local approximation allows us to simplify the integral $I_{\rm ion}(t)$ appearing in Eq. (34). Taking into account that $\Sigma^{<}_{\rm ion} = 0$ we have

$$I_{\rm ion}(t) = \int_{-\infty}^{t} dt'\,\Sigma^{>}_{\rm ion}(t,t')G^{<}(t',t) = \Gamma(t)\rho(t). \quad (41)$$

Inserting this result into Eq. (34) we finally obtain

$$-i\frac{d}{dt}\rho(t) + [h_{\rm HF}(t),\rho(t)] - i\{\Gamma(t),\rho(t)\} = iI(t) - \text{H.c.}, \quad (42)$$

where the curly brackets signify an anticommutator. Equation (42) constitutes the generalization of the NEGF + GKBA formalism to open systems [48].

VI. KRYPTON

We apply the formalism of the previous section to address a retardation effect observed by Goulielmakis *et al.* [34] in the TPA spectrum of a krypton gas. In the experiment a strong pump is shone on the gas, electrons from the $4p$ shell are expelled, and an admixture of Kr atoms and Kr^{n+} ions, with $n = 1,2,3,\ldots$, is formed. The admixture is subsequently probed with an ultrafast pulse, thus inducing transitions from the $3d$ to the $4p$ shell. The main focus in Ref. [34] is on the coherent oscillations [12,13,15] of the peak intensities of the Kr^{1+} ion as a function of the pump-probe delay τ. However, the experimental TPA spectrum reveals another interesting feature as a function of τ. The absorption peaks of Kr^{2+} develop after the absorption peaks of Kr^{1+}, implying that it is faster to expel one electron than two electrons. To reproduce this retardation effect theoretically a formalism for the TPA spectrum of an *evolving admixture* is needed. The NEGF + GKBA approach is, in principle, suitable for this purpose. As we shall see, important qualitative aspects of the admixture are intimately related to the diagrammatic structure of the self-energy.

The Kr gas is ionized by a few-cycle NIR pump $\mathbf{E}(\ell t) = (E(t),0,0)$, with $E(t) = E_0\sin^2(\pi t/\Delta_P)\sin(\omega_P t)$ for $0 < t < \Delta_P$. The experimental pump intensity is $\mathcal{I}_0 = 7\times10^{14}\mathrm{W/cm^2}$, corresponding to an electric field $E_0 = \sqrt{2\mathcal{I}_0/c\epsilon_0} = 7.2\times10^{10}$ V/m, the duration of the pump pulse is $\Delta_P \sim 7.6$ fs, and the NIR frequency is $\omega_P \sim 1.65$ eV. After a time τ the Kr admixture is probed with an extreme ultraviolet attosecond pulse $\mathbf{e}(\ell t) = (e(t),0,0)$, with $e(t) = e_0\sin^2(\pi(t-\tilde{\tau})/\Delta_p)\sin(\omega_p(t-\tilde{\tau}))$ for $\tilde{\tau} < t < \tilde{\tau}+\Delta_p$. Here $\tau = \tilde{\tau} - (\Delta_P-\Delta_p)/2$ is the time distance between the maximum of the pump and that of the probe pulses. The probe pulse has duration $\Delta_p \sim 150$ as, it is centered at frequency $\omega_p = 80$ eV, and it has an intensity $\mathrm{i}_0 \sim 10^{11}\mathrm{W/cm^2}$, which corresponds to an electric field $e_0 = 8.6\times10^8$ V/m. We discard the dressing of the probe field and solve the equation of motion for ρ with $\boldsymbol{\mathcal{E}} = \mathbf{e}$.

The one- and two-electron integrals as well as the dipole matrix elements have been calculated with the SMILES package [64,65] using the 66 Slater-type orbital basis functions taken from Ref. [67]. As we are not interested in the coherent oscillations of the peak intensities, we do not include the spin-orbit coupling responsible for the splitting of the $4p$ and $3d$ orbitals. Thus we should expect one main absorption peak *per ion*, corresponding to transitions from the $4p$ to the $3d$ shell. We find 18 HF states with an energy below zero. The remaining HF states are used to construct the ionization self-energy according to Eq. (37). The simulations show that electrons are essentially removed from the $4p$ shell, in agreement with the analysis in Ref. [34]. In Fig. 7 we display the transient ionization yield, i.e., the expelled charge per spin, during the action of the pump. The charge is expelled in pockets at a rate of twice the frequency of the laser pulse, in agreement with CI calculations [12,34]. Interestingly, the HF and 2B yields are indistinguishable. The situation is drastically different for the TPA spectrum, with the 2B approximation performing much better than the HF one (see below). Whether the absorption onset of Kr^{1+} is earlier than the absorption onset of Kr^{2+} is the central issue addressed below.

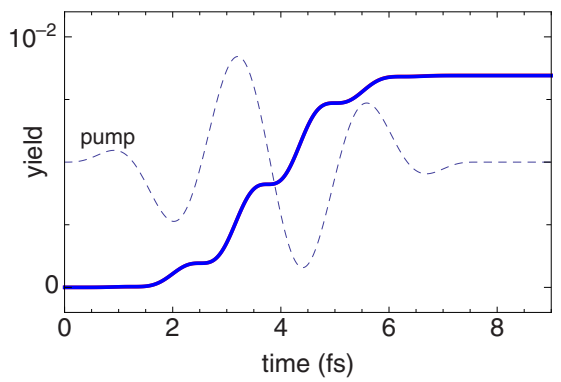

FIG. 7. (Color online) Transient ionization yield per spin (solid line) in the HF and 2B (indistinguishable) and amplitude of the pump pulse (dashed line) in arbitrary units.

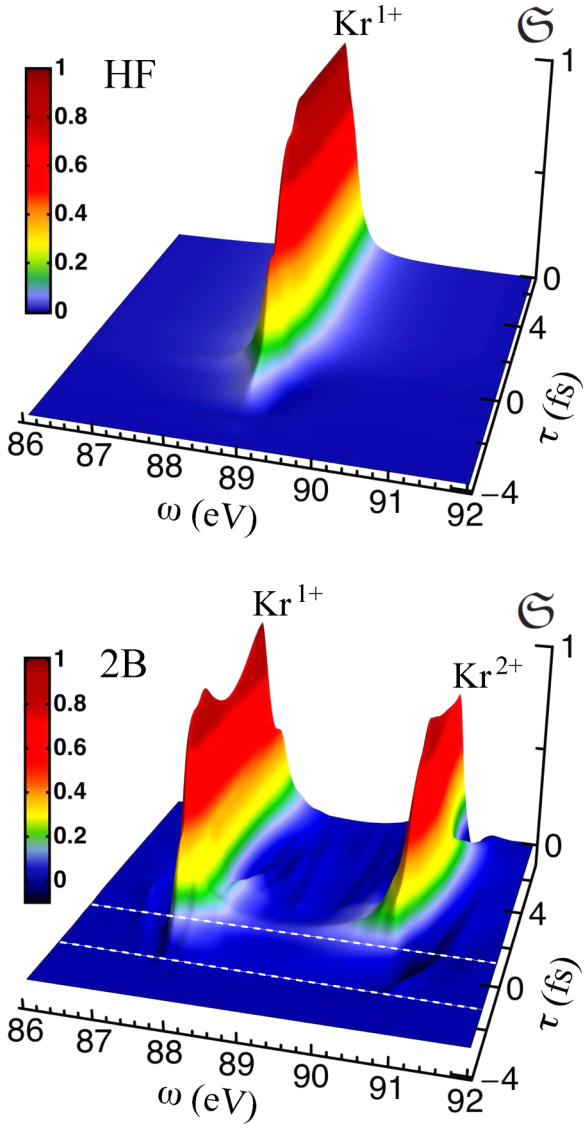

FIG. 8. (Color online) TPA spectrum (normalized to the maximum height) of a krypton gas in the HF (top) and 2B (bottom) approximations. Dashed (white) lines in the bottom panel are guides for the eye, to better visualize the retardation effect. Pump and probe pulses are given in the text.

In the upper panel in Fig. 8 we report the TPA spectrum of the Kr admixture in the HF approximation. We have propagated the system for ∼50 fs after the action of the probe with a time step $\Delta t = 0.0025$ fs (corresponding to 20 000 time steps) and then broadened the Fourier transform of $\mathbf{d}_p(t)$ by 0.8 eV to account for the experimental resolution. The result is extremely disappointing. The HF TPA spectrum consists of one doublet (merged in Fig. 8 into one single line shape due to the broadening), with a simultaneous rise in both peaks. The peaks correspond to transitions from the $3d$ shell to either the $4p_x$ orbital or the $4p_{y,z}$ orbitals. In fact, these transitions are nondegenerate in the HF approximation. As the pump is polarized along x the $4p_x$ orbital loses more charge than the $4p_{y,z}$ orbitals, thereby breaking the degeneracy (albeit only slightly). Even more noteworthy, however, is the absence of spectral structures due to absorption of multiply ionized Kr atoms. The numerical simulation has been repeated with pump fields of different frequencies and intensities but no sign of other absorption peaks has been observed. The first important conclusion of this preliminary study is that the appearance of absorption peaks in multiply ionized Kr atoms is a *correlation effect*.

We then included correlation effects at the level of the Markovian 2B approximation but the outcome did not change (not shown). The main difference between the HF and the Markovian 2B spectra is an overall frequency shift. The numerical evidence accumulated so far leads us to conjecture that any time-local approximation (no memory) to the self-energy is doomed to fail. We mention that the equation of motion for ρ with a time-local Σ has the same mathematical structure as the TDDFT equations at the level of the ALDA. Hence, TDDFT spectra at the ALDA level would also fail to capture the absorption peaks of multiply ionized atoms. The second important conclusion is that static correlation effects are not enough.

Dynamical correlation effects are contained in the full (nonlocal in time) 2B self-energy. We have solved the equations of motion for ρ with the collision integral of Eq. (26). The TPA spectrum is shown in the lower panel in Fig. 8. We clearly distinguish two structures corresponding to the TPA spectrum of Kr^{1+} and Kr^{2+}. In fact, the energy gap between the structures is consistent with the ∼3-eV experimental gap between these two ions [68]. Remarkably, the high-energy structure develops ∼3 fs after the low-energy one. This is the aforementioned retardation effect, which we have just proved to be within reach of the NEGF + GKBA approach. Furthermore, the obtained delay is commensurate with the 5-fs delay observed in experiments. A self-energy that is nonlocal in time is crucial for the appropriate description of the Kr (and probably of any other) evolving admixture.

Although the 2B approximation represents a noticeable improvement over time-local approximations, there remains one issue to address. The experimental TPA spectrum contains small absorption peaks attributable to transitions in the Kr^{3+} ion. We have not been able to see these structures within the 2B approximation. Although we are not aware of any formal result relating the possibility of describing multiply ionized atoms to the diagrammatic structure of the self-energy, we observe that the kernel $\delta\Sigma/\delta G$ contains at most one particle-hole excitation in the HF and two particle-hole excitations in the 2B approximation. It is therefore tempting to argue that in order to observe the absorption peaks of Kr^{n+} the kernel $\delta\Sigma/\delta G$ should contain at least n particle-hole excitations [31,69], which implies that Σ should contain diagrams of order at least n in the interaction. Finding a general solution to this problem would certainly be valuable and contribute to advancing the understanding of many-body diagrammatic theories.

VII. CONCLUSIONS

We have introduced an NEGF + GKBA approach to TPA experiments suitable for pump fields of arbitrary strength, frequency, and duration and for any delay between pump and probe pulses (hence also for delays in the overlapping regime). The size of the arrays in NEGF calculations

scales quadratically with the number of basis functions. The Coulomb interaction between electrons is included diagrammatically through the correlation self-energy and the possibility of ionization can be described through the ionization self-energy.

The approach has been benchmarked against the TPA spectrum of He reported in Ref. [11]. Helium is a weakly correlated system and all self-energy approximations have been shown to agree with the CI results. We have provided a simple yet rigorous explanation for the bending of the AT absorption peaks and derived a useful formula for fitting the experimental TPA spectra. We have also addressed the exponential damping of the probe-induced dipole and related it to the thickness and density of the gas.

A more severe test of the NEGF + GKBA approach is the TPA spectrum of Kr reported in Ref. [34]. We have shown that for a proper description of the evolving admixture of Kr ions, the self-energy should have *memory*. This is not the case for the HF and Markovian 2B self-energies, which yield the TPA spectrum of a pure Kr^{1+} ion. We argue that the situation does not change in TDDFT with ALDA exchange-correlation potentials. On the contrary, the full 2B self-energy leads to a second structure in the TPA spectrum that is assigned to Kr^{2+} and that develops about 2–3 fs after the first, in fair agreement with the experiment. More theoretical and numerical work is needed to understand the relation between self-energy diagrams and the emergence of absorption peaks due to multiply ionized atoms.

ACKNOWLEDGMENTS

We thank Rafael López for providing us with the SMILES package and Stefan Kurth for useful discussions. We would further like to thank the CSC-IT center for science in Espoo, Finland, for computing resources. E.P. and G.S. acknowledge funding by MIUR FIRB Grant No. RBFR12SW0J. R.v.L. thanks the Academy of Finland for support.

APPENDIX: THE EMBEDDED GKBA EQUATION FOR ρ

The lesser and greater Green's functions follow from the Keldysh Green's function $G(z,z')$, with arguments z and z' on the Keldysh contour. In particular, $G^<$ ($G^>$) is the Keldysh G with the first (second) contour argument on the forward branch and the second (first) contour argument on the backward branch. The Keldysh G satisfies the equations of motion [31] (in matrix form),

$$\left[i\frac{d}{dz} - h_{\rm HF}(z)\right]G(z,z') = \delta(z,z') + \int d\bar{z}\,\Sigma(z,\bar{z})G(\bar{z},z'), \tag{A1}$$

$$G(z,z')\left[-i\frac{\overleftarrow{d}}{dz'} - h_{\rm HF}(z')\right] = \delta(z,z') + \int d\bar{z}\,G(z,\bar{z})\Sigma(\bar{z},z'), \tag{A2}$$

where the integral is over the Keldysh contour. Choosing z on the backward branch and z' on the forward branch, and applying the Langreth rules, we obtain the equations of motion for $G^<$:

$$\left[i\frac{d}{dt} - h_{\rm HF}(t)\right]G^<(t,t') = \int d\bar{t}\,\Sigma^{\rm R}(t,\bar{t})G^<(\bar{t},t') + \int d\bar{t}\,\Sigma^<(t,\bar{t})G^{\rm A}(\bar{t},t'), \tag{A3}$$

$$G^<(t,t')\left[-i\frac{\overleftarrow{d}}{dt'} - h_{\rm HF}(t')\right] = \int d\bar{t}\,G^{\rm R}(t,\bar{t})\Sigma^<(\bar{t},t') + \int d\bar{t}\,G^<(t,\bar{t})\Sigma^{\rm A}(\bar{t},t'). \tag{A4}$$

The upper indices "R" and "A" signify retarded and advanced functions, respectively. These are defined according to

$$F^{\rm R/A}(t,t') = \pm\theta(\pm t \mp t')[F^>(t,t') - F^<(t,t')]. \tag{A5}$$

Subtracting Eq. (A4) from Eq. (A3) and setting $t' = t$, we find the equation of motion, Eq. (20), for the density matrix $\rho(t) = -iG^<(t,t)$.

Let us work in the HF basis $\{\psi_\mu\}$ of the equilibrium system and write $\rho_{\mu\nu}(t) = \delta_{\mu\nu}n_\mu + \delta\rho_{\mu\nu}(t)$. In the same basis the HF Hamiltonian in Eq. (21) reads

$$h_{{\rm HF},\mu\nu}(t) = \tilde{h}_{{\rm HF},\mu\nu}(t) + \boldsymbol{\mathcal{E}}(t)\cdot\mathbf{d}_{\mu\nu}, \tag{A6}$$

with

$$\tilde{h}_{{\rm HF},\mu\nu}(t) = h_{\mu\nu} + \sum_{\alpha\beta} w_{\mu\alpha\beta\nu}\rho_{\beta\alpha}(t) = \delta_{\mu\nu}\epsilon_\mu + \sum_{\alpha\beta} w_{\mu\alpha\beta\nu}\delta\rho_{\beta\alpha}(t). \tag{A7}$$

The HF states can be grouped according to their energies: if $\epsilon_\mu < 0$, then ψ_μ is a bound state; otherwise, ψ_μ is a continuum state. We assume that the two-electron integrals $v_{\mu\alpha\beta\nu}$ with at least one index in the continuum are negligible and set them to 0. Consequently, $w_{\mu\alpha\beta\nu}$ with at least one index in the continuum vanishes too. Let us represent a matrix $\mathcal{M}$ in the HF basis as

$$\mathcal{M} = \begin{pmatrix} \mathcal{M}^{bb} & \mathcal{M}^{bc} \\ \mathcal{M}^{bc} & \mathcal{M}^{cc} \end{pmatrix}, \tag{A8}$$

where in $\mathcal{M}^{bb}_{\mu\nu}$ both indices run over the bound states, in $\mathcal{M}^{bc}_{\mu\nu}$ the first index runs over the bound states and the second index over the continuum states, and so on. Then the HF Hamiltonian has the block structure

$$h_{\rm HF} = \begin{pmatrix} h^{bb}_{\rm HF} & \boldsymbol{\mathcal{E}}\cdot\mathbf{d}^{bc} \\ \boldsymbol{\mathcal{E}}\cdot\mathbf{d}^{cb} & h^{cc}_{\rm HF} \end{pmatrix}, \tag{A9}$$

where we took into account that $\tilde{h}^{bc}_{\rm HF} = 0$ [see Eq. (A7)]. Similarly, we infer that the block structure of the correlation self-energy is

$$\Sigma = \begin{pmatrix} \Sigma^{bb} & 0 \\ 0 & 0 \end{pmatrix}. \tag{A10}$$

We can make use of the block structure of $h_{\rm HF}$ and Σ to simplify the equations of motion for the Keldysh G. In the bound-bound sector Eq. (A1) reads

$$\left[i\frac{d}{dz} - h^{bb}_{\rm HF}(z)\right]G^{bb}(z,z') - [\boldsymbol{\mathcal{E}}(z)\cdot\mathbf{d}^{bc}]G^{cb}(z,z') = \delta(z,z') + \int d\bar{z}\,\Sigma^{bb}(z,\bar{z})G^{bb}(\bar{z},z'), \tag{A11}$$

whereas in the continuum-bound sector the same equation reads

$$\left[i\frac{d}{dz} - h^{cc}_{\rm HF}(z)\right]G^{cb}(z,z') - [\boldsymbol{\mathcal{E}}(z)\cdot\mathbf{d}^{cb}]G^{bb}(z,z') = 0. \tag{A12}$$

We define the continuum (noninteracting) Green's function g^{cc} as the solution of

$$\left[i\frac{d}{dz} - h^{cc}_{\rm HF}(z)\right]g^{cc}(z,z') = \delta(z,z') \tag{A13}$$

and rewrite Eq. (A12) in integral form,

$$G^{cb}(z,z') = \int d\bar{z}\,g^{cc}(z,\bar{z})[\boldsymbol{\mathcal{E}}(\bar{z})\cdot\mathbf{d}^{cb}]G^{bb}(\bar{z},z'). \tag{A14}$$

Inserting Eq. (A14) into Eq. (A11) we find

$$\left[i\frac{d}{dz} - h^{bb}_{\rm HF}(z)\right]G^{bb}(z,z') = \delta(z,z') + d\bar{z}\left[\Sigma^{bb}(z,\bar{z}) + \Sigma^{bb}_{\rm ion}(z,\bar{z})\right]G^{bb}(\bar{z},z'), \tag{A15}$$

with the ionization self-energy defined according to

$$\Sigma^{bb}_{\rm ion}(z,z') = [\boldsymbol{\mathcal{E}}(z)\cdot\mathbf{d}^{bc}]g^{cc}(z,z')[\boldsymbol{\mathcal{E}}(z')\cdot\mathbf{d}^{cb}]. \tag{A16}$$

Thus, the continuum states can be downfolded in an exact way into an effective equation for G^{bb}. A similar equation can be derived starting from Eq. (A2) and reads

$$G^{bb}(z,z')\left[-i\frac{\overleftarrow{d}}{dz'} - h^{bb}_{\rm HF}(z')\right] = \delta(z,z')\int d\bar{z}\,G^{bb}(z,\bar{z})\left[\Sigma^{bb}(\bar{z},z') + \Sigma^{bb}_{\rm ion}(\bar{z},z')\right]. \tag{A17}$$

Below we use Eqs. (A15) and (A17) to generate an equation for the density matrix in the bound-bound sector. To lighten the notation we omit the superscript indices "*bb*," so a matrix with no superscripts is a matrix in the bound-bound sector.

Comparing Eqs. (A15) and (A17) with Eqs. (A1) and (A2) we deduce that the equations of motion for $G^<$ are the same as Eqs. (A3) and (A4) except that the correlation self-energy is replaced by $\Sigma + \Sigma_{\rm ion}$. Therefore, the equation of motion for ρ is the same as Eq. (20) except that the collision integral is calculated with $\Sigma^{\lessgtr} + \Sigma^{\lessgtr}_{\rm ion}$. From Eq. (A13) we have

$$g^{cc,\lessgtr}_{\mu\nu}(t,t') = -i\sum_{\alpha\in c}\mathcal{U}^{cc}_{\mu\alpha}(t)\,n^{\lessgtr}_{\alpha}\,[\mathcal{U}^{cc}(t')]^{\dagger}_{\alpha\nu}, \tag{A18}$$

where $\mathcal{U}^{cc}(t) = T[e^{-i\int_0^t dt' h^{cc}_{\rm HF}(t')}]$ is the evolution operator in the continuum sector, whereas $n^<_\alpha = n_\alpha$ and $n^>_\alpha = 1 - n_\alpha$. For α in the continuum we have $\epsilon_\alpha > 0 > \epsilon_{\rm F}$ and hence $n^<_\alpha = 0$ (which implies $g^{cc,<} = 0$) and $n^>_\alpha = 1$. The evolution operator takes a very simple form if we ignore the effect of the pump between continuum states, i.e., if we approximate $\mathbf{d}^{cc} \approx 0$. In this case $h^{cc}_{{\rm HF},\mu\nu} = \delta_{\mu\nu}\epsilon_\mu$ [see Eqs. (A6) and (A7)], and hence

$$g^{cc,>}_{\mu\nu}(t,t') = -i\delta_{\mu\nu}e^{-i\epsilon_\mu(t-t')}. \tag{A19}$$

From Eq. (A16) it follows that the greater ionization self-energy is

$$\Sigma^{>}_{{\rm ion},\mu\nu}(t,t') = -i\sum_{\alpha}\left[\boldsymbol{\mathcal{E}}(t)\cdot\mathbf{d}^{bc}_{\mu\alpha}\right]e^{-i\epsilon_\alpha(t-t')}\left[\boldsymbol{\mathcal{E}}(t')\cdot\mathbf{d}^{cb}_{\alpha\nu}\right], \tag{A20}$$

which agrees with Eqs. (35) and (36).

[1] F. Krausz and M. Ivanov, Rev. Mod. Phys. **81**, 163 (2009).
[2] R. Berera, R. van Grondelleand, and J. T. M. Kennis, Photosynth. Res. **101**, 105 (2009).
[3] G. Sansone, T. Pfeifer, K. Simeonidis, and A. I. Kuleff, Chem. Phys. Chem. **13**, 661 (2012).
[4] L. Gallmann, J. Herrmann, R. Locher, M. Sabbar, A. Ludwig, M. Lucchini, and U. Keller, Mol. Phys. **111**, 2243 (2013).
[5] A. I. Kuleff and L. S. Cederbaum, J. Phys. B: At. Mol. Opt. Phys. **47**, 124002 (2014).
[6] M. B. Gaarde, C. Buth, J. L. Tate, and K. J. Schafer, Phys. Rev. A **83**, 013419 (2011).
[7] S. Pabst, L. Greenman, P. J. Ho, D. A. Mazziotti, and R. Santra, Phys. Rev. Lett. **106**, 053003 (2011).
[8] W.-C. Chu and C. D. Lin, Phys. Rev. A **85**, 013409 (2012).
[9] M. Tarana and C. H. Greene, Phys. Rev. A **85**, 013411 (2012).
[10] S. Pabst, A. Sytcheva, A. Moulet, A. Wirth, E. Goulielmakis, and R. Santra, Phys. Rev. A **86**, 063411 (2012).
[11] A. N. Pfeiffer, M. J. Bell, A. R. Beck, H. Mashiko, D. M. Neumark, and S. R. Leone, Phys. Rev. A **88**, 051402 (2013).
[12] N. Rohringer and R. Santra, Phys. Rev. A **79**, 053402 (2009).
[13] R. Santra, V. S. Yakovlev, T. Pfeifer, and Z.-H. Loh, Phys. Rev. A **83**, 033405 (2011).
[14] J. C. Baggesen, E. Lindroth, and L. B. Madsen, Phys. Rev. A **85**, 013415 (2012).
[15] E. Perfetto and G. Stefanucci, Phys. Rev. A **91**, 033416 (2015).
[16] U. De Giovannini, G. Brunetto, A. Castro, J. Walkenhorst, and A. Rubio, Chem. Phys. Chem. **14**, 1363 (2013).
[17] C. Neidel, J. Klei, C.-H. Yang, A. Rouzée, M. J. J. Vrakking, K. Klünder, M. Miranda, C. L. Arnold, T. Fordell, A. L'Huillier *et al.*, Phys. Rev. Lett. **111**, 033001 (2013).
[18] S. M. Falke, C. A. Rozzi, D. Brida, M. Maiuri, M. Amato, E. Sommer, A. D. Sio, A. Rubio, G. Cerullo, E. Molinari *et al.*, Science **344**, 1001 (2014).
[19] C. A. Rozzi, S. M. Falke, N. Spallanzani, A. Rubio, E. Molinari, D. Brida, M. Maiuri, G. Cerullo, H. Schramm, J. Christoffers *et al.*, Nat. Commun. **4**, 1602 (2013).
[20] N. T. Maitra, F. Zhang, R. J. Cave, and K. Burke, J. Chem. Phys. **120**, 5932 (2004).
[21] S. Kümmel and L. Kronik, Rev. Mod. Phys. **80**, 3 (2008).
[22] O. Gritsenko and E. J. Baerends, J. Chem. Phys. **121**, 655 (2004).

[23] N. T. Maitra, J. Chem. Phys. **122**, 234104 (2005).
[24] N. T. Maitra and D. G. Tempel, J. Chem. Phys. **125**, 184111 (2006).
[25] J. B. Neaton, M. S. Hybertsen, and S. G. Louie, Phys. Rev. Lett. **97**, 216405 (2006).
[26] A. M. Souza, I. Rungger, C. D. Pemmaraju, U. Schwingenschloegl, and S. Sanvito, Phys. Rev. B **88**, 165112 (2013).
[27] G. Stefanucci and S. Kurth, Phys. Rev. Lett. **107**, 216401 (2011).
[28] S. Kurth and G. Stefanucci, Phys. Rev. Lett. **111**, 030601 (2013).
[29] L. P. Kadanoff and G. Baym, *Quantum Statistical Mechanics* (W. A. Benjamin, New York, 1962).
[30] H. Haug and A.-P. Jauho, *Quantum Kinetics in Transport and Optics of Semiconductors* (Springer, Berlin, 2007).
[31] G. Stefanucci and R. van Leeuwen, *Nonequilibrium Many-Body Theory of Quantum Systems: A Modern Introduction* (Cambridge University Press, Cambridge, UK, 2013).
[32] K. Balzer and M. Bonitz, *Nonequilibrium Green's Functions Approach to Inhomogeneous Systems*, Lecture Notes in Physics, Vol. 867 (Springer-Verlag, Berlin, Heidelberg, 2013).
[33] E. Perfetto, D. Sangalli, A. Marini, and G. Stefanucci, arXiv:1507.01786.
[34] E. Goulielmakis, Z. Loh, A. Wirth, R. Santra, N. Rohringer, V. S. Yakovlev, S. Zherebtsov, T. Pfeifer, A. M. Azzeer, M. F. Kling *et al.*, Nature **466**, 739 (2010).
[35] P. Lipavský, V. Špička, and B. Velický, Phys. Rev. B **34**, 6933 (1986).
[36] M. Bonitz, D. Kremp, D. C. Scott, R. Binder, W. D. Kraeft, and H. S. Köhler, J. Phys.: Condens. Matter **8**, 6057 (1996).
[37] N. H. Kwong, M. Bonitz, R. Binder, and H. S. Köhler, Phys. Status Solidi B **206**, 197 (1998).
[38] H. Haug, Phys. Status Solidi B **173**, 139 (1992).
[39] R. Binder, H. S. Köhler, M. Bonitz, and N. Kwong, Phys. Rev. B **55**, 5110 (1997).
[40] M. Bonitz, D. Semkat, and H. Haug, Eur. Phys. J. B **9**, 209 (1999).
[41] P. Gartner, L. Bányai, and H. Haug, Phys. Rev. B **60**, 14234 (1999).
[42] Q. T. Vu and H. Haug, Phys. Rev. B **62**, 7179 (2000).
[43] A. Marini, J. Phys: Conf. Proc. **427**, 012003 (2013).
[44] D. Sangalli and A. Marini, arXiv:1409.1706.
[45] K. Balzer, S. Hermanns, and M. Bonitz, J. Phys.: Conf. Ser. **427**, 012006 (2013).
[46] M. Bonitz, K. Balzer, and S. Hermanns, Contrib. Plasma Phys. **53**, 778 (2013).
[47] S. Hermanns, N. Schlünzen, and M. Bonitz, Phys. Rev. B **90**, 125111 (2014).
[48] S. Latini, E. Perfetto, A.-M. Uimonen, R. van Leeuwen, and G. Stefanucci, Phys. Rev. B **89**, 075306 (2014).
[49] N. E. Dahlen and R. van Leeuwen, Phys. Rev. Lett. **98**, 153004 (2007).
[50] P. Myöhänen, A. Stan, G. Stefanucci, and R. van Leeuwen, Europhys. Lett. **84**, 67001 (2008).
[51] P. Myöhänen, A. Stan, G. Stefanucci, and R. van Leeuwen, Phys. Rev. B **80**, 115107 (2009).
[52] K. Balzer, M. Bonitz, R. van Leeuwen, A. Stan, and N. E. Dahlen, Phys. Rev. B **79**, 245306 (2009).
[53] M. P. von Friesen, C. Verdozzi, and C.-O. Almbladh, Phys. Rev. Lett. **103**, 176404 (2009).
[54] K. Balzer, S. Bauch, and M. Bonitz, Phys. Rev. A **81**, 022510 (2010).
[55] K. Balzer, S. Bauch, and M. Bonitz, Phys. Rev. A **82**, 033427 (2010).
[56] N. Schlünzen, S. Hermanns, M. Bonitz, and C. Verdozzi, arXiv:1508.02947 [cond-mat].
[57] Y. Bar Lev and D. R. Reichman, arXiv:1508.05391 [cond-mat].
[58] P. Ranitovic, X. M. Tong, C. W. Hogle, X. Zhou, Y. Liu, N. Toshima, M. M. Murnane, and H. C. Kapteyn, Phys. Rev. Lett. **106**, 193008 (2011).
[59] A. N. Pfeiffer and S. R. Leone, Phys. Rev. A **85**, 053422 (2012).
[60] S. Chen, M. J. Bell, A. R. Beck, H. Mashiko, M. Wu, A. N. Pfeiffer, M. B. Gaarde, D. M. Neumark, S. R. Leone, and K. J. Schafer, Phys. Rev. A **86**, 063408 (2012).
[61] S. Chen, M. Wu, M. B. Gaarde, and K. J. Schafer, Phys. Rev. A **87**, 033408 (2013).
[62] M. Wu, S. Chen, M. B. Gaarde, and K. J. Schafer, Phys. Rev. A **88**, 043416 (2013).
[63] M. Chini, X. Wang, Y. Cheng, and Z. Chang, J. Phys. B: At. Mol. Opt. Phys. **47**, 124009 (2014).
[64] J. Fernández Rico, I. Ema, R. López, G. Ramírez, and K. Ishida, in *Recent Advances in Computational Chemistry: Molecular Integrals over Slater Orbitals*, edited by T. Ozdogan and M. B. Ruiz (Transworld Research Network, Trivandrum, India, 2008), p. 145.
[65] J. F. Rico, R. Lopez, G. Ramirez, and I. Ema, J. Comput. Chem. **25**, 1987 (2004).
[66] C.-T. Liao, A. Sandhu, S. Camp, K. J. Schafer, and M. B. Gaarde, Phys. Rev. Lett. **114**, 143002 (2015).
[67] C. F. Bunge, J. A. Barrientos, and A. V. Bunge, At. Data Nucl. Data Tables **53**, 113 (1993).
[68] Similarly to the He case, the absolute position of the peaks is shifted with respect to experiments.
[69] N. Säkkinen, M. Manninen, and R. van Leeuwen, New J. Phys. **14**, 013032 (2012).